



Imene Laoufi · Amina Attia · Fouad Bourada ·
Abdelouahed Tounsi · Abdeldjebbar Tounsi ·
Khaled Mohamed Khedher · Mohamed Abdelaziz Salem ·
Murat Yaylaci

Stability analysis of porous FG sandwich plates under thermomechanical loads via integral HySDT

Received: 30 March 2024 / Accepted: 17 July 2024

© The Author(s), under exclusive licence to Springer-Verlag GmbH Germany, part of Springer Nature 2024

Abstract The thermomechanical buckling of imperfect sandwich plates made of functionally graded material (FGM) is addressed analytically in this study. A novel hyperbolic four-variable integral shear deformation theory is used to arrive at the solution. Sandwich plates come in two varieties: the first with homogeneous core and FG face sheets and the second with the opposite. The displacement field is constructed using undetermined integrals in order to reduce the number of unknown variables which consequently reduces the calculation time unlike other similar theories. The proposed model does not require a shear correction factor and ensures the free-stress at the upper and lower surfaces of structure. The materials properties of the structure are computed via power-law function with considering the porosity effect which may appear during manufacturing due to the difference in solidification temperature of the constituents (ceramic/metal). Four types of geometric imperfection are examined with even, uneven, logarithmic uneven and linear uneven distributions. On the basis of the minimal total potential energy concept, the governing equations are developed. The Navier's method is used to solve these equations for simply supported plates. The results of simply supported FGM sandwich plates' critical buckling load and temperature increment are contrasted with the available solutions

I. Laoufi

Department of Civil Engineering and Publics Works, Innovative Materials Laboratory and Renewable Energies, University of Relizane, Relizane, Algeria

A. Attia

Engineering and Sustainable Development Laboratory, Department of Civil Engineering and Public Works, Faculty of Science and Technology, University of Ain Temouchent, Ain Temouchent, Algeria

F. Bourada · A. Tounsi

Material and Hydrology Laboratory, Department of Civil Engineering, Faculty of Technology, University of Sidi Bel Abbès, Sidi Bel Abbès, Algeria

A. Tounsi

Department of Civil and Environmental Engineering, King Fahd University of Petroleum and Minerals, 31261 Dhahran, Eastern Province, Saudi Arabia

A. Tounsi (✉)

Department of Mechanical Engineering, Faculty of Science and Technology, University of Relizane, Relizane, Algeria
e-mail: tounsi_abdeldjebbar@yahoo.com

K. M. Khedher

Department of Civil Engineering, College of Engineering, King Khalid University, 61421 Abha, Saudi Arabia

M. A. Salem

Department of Mechanical Engineering, College of Engineering, King Khalid University, 61421 Abha, Saudi Arabia

M. Yaylaci

Department of Civil Engineering, Recep Tayyip Erdogan University, 53100 Rize, Turkey

M. Yaylaci

Faculty of Turgut Kiran Maritime, Recep Tayyip Erdogan University, 53900 Rize, Turkey

in the literature. Even, uneven, linear uneven and logarithmic uneven models of distribution are taken into consideration and studied in order to incorporate porosity in the FG face sheet and core. Investigation is conducted into the effects of layer thickness, porosity models, porosity coefficients and geometrical parameters on the thermomechanical buckling response of imperfect FG sandwich plates.

Keywords FG sandwich plates · Integral shear deformation theory · Thermomechanical buckling · Porosity effect

1 Introduction

Sandwich structures are widely used in the aircraft, aerospace, flexible electronics and biomedical fields due to their many advantages, including as their light weight and excellent bending stiffness [1]. A typical sandwich structure consists of a homogeneous core sandwiched between two homogenous face sheets. Sandwich structures have recently become even more appealing as a result of the development of materials that are not homogeneous, functionally graded materials (FGMs) for example, Garg et al. [2]. FGMs improve sandwich structures' mechanical and thermal properties by reducing interlaminar stresses and thermal stresses as choices for the face sheets and/or the core [3–11]. Two forms of FG sandwich structures are primarily covered in the literature: Type-A sandwich structures have FGM face sheets and a homogeneous core [12–16], whereas type-B sandwich structures do the opposite [17–19]. FGM sandwich structures provide exceptional potential in many engineering domains, such as submarines, return capsules, planetary exploratory landers and so on [20, 21]. They combine the two benefits of sandwich structures and FGMs. Researchers have looked into the buckling behavior of FG sandwich constructions as one of the important failure types. However, the majority among them limited to FGM sandwich plates when subjected to thermal load or mechanical load [22–35]. There are not many publications that take mechanical and thermal load into account. For an accurate prediction of the buckling issue, it is crucial to take both into account because in actuality, sandwich plates made of FGMs are regularly subjected to simultaneous mechanical and thermal loads. In order to investigate the type-A FG sandwich plate's buckle under mechanical load and uniform temperature escalation, the Galerkin-differential quadrature method is used by Yang et al. [36] utilizing a high-order equivalent-single-layer (ESL) theory. Shen and his colleagues [37, 38] investigated the buckling and post-buckling of type-A FG sandwich plates under thermal and mechanical loads using a method called two-step perturbation. Yaghoobi and Yaghoobi [39] studied the effects of both thermal and mechanical buckling of type-A FG sandwich plates supported by an elastic base using a first-order ESL theory. Using a first-order ESL theory, Tung [40] performed a thermomechanical post-buckling analysis of FG sandwich plates under mechanical load and uniform temperature rise.

Inside the plate made of FGMs, micro-voids or porosities are created during the production. Different temperatures of solidification for the components that make up FGMs result in the creation of porosity or micro-voids inside the plate for the period of manufacturing. Porosities or micro-voids in the materials diminish the plate's mechanical rigidity, which could result in structural failure [41–43]. Investigating the structural response of porous FG plates requires taking into account the plate's porosity. To determine the structural response of porous FG sandwich models, a variety of even and uneven porosity models have been proposed and developed [44–46]. By taking into account in-surface curvilinear motions, Karami and Ghayesh [47] investigate the vibrations of sandwich micro-shells with functionally graded porous face sheets. Hadji et al. [48] have analyzed the naturel frequency of the natural frequency of the sandwich FG-plate comprised the micro-voids in the face sheets and reposed on Winkler–Pasternak foundation with the help of the kinematic of the third-order shear deformation theory. Ghazwani et al. [49] examined the impact of various distribution of the porosity on the vibrational response of the FG-nanobeams based on Hamilton's principle and Eringen's theory. The trigonometric shear deformation theory (TrSDT) is used by Avcar et al. [50] to examine the natural frequency of perfect/imperfect FG sandwich beam reposed on two-parameter elastic foundation. The analysis is performed for various edges boundary conditions. Avcar et al. [51] examined the flexural behaviors of FG sandwich beam with including the porosity effect by modifying the rule of mixtures of material. The analysis has performed via hyperbolic shear deformation theory. Also, the dynamic analysis of the FG- sandwich beams is investigated based on the trigonometric shear deformation theory by Avcar et al. [52]. The effect of the porosity volume fractions with different types of porosity distribution pattern is also discussed. The effects of the boundary conditions, porosity volume fraction, lay-up scheme and side-to-thickness ratio on the vibrational analysis of FG sandwich plates are studied analytical by Hadji and Avcar [53] by employing the hyperbolic shear displacement theory. Also, recent various works are published to investigate the impact of the geometric imperfection on the structures responses as [54–57].

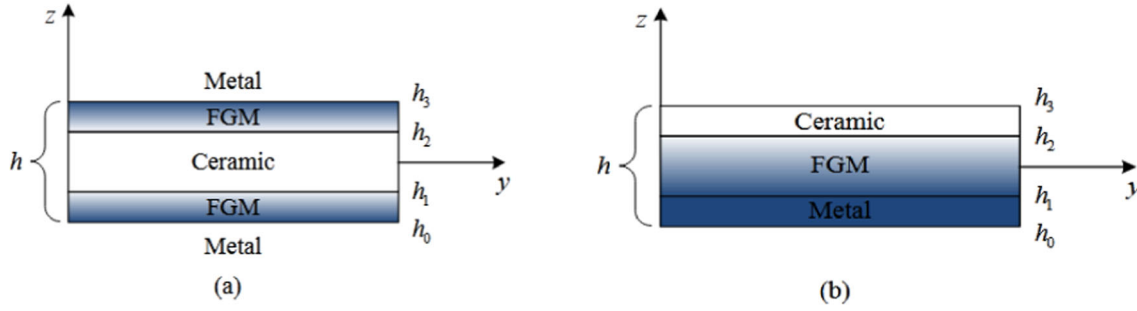


Fig. 1 Sandwich plates with FGM come in two varieties **a** FG face sheets and a homogenous core characterize type A. **b** FG core and homogenous face-sheets for type-B

The literature research revealed that the scant amount of information that is currently accessible is insufficient for supplying a thorough familiarity with the behavior that buckles FG sandwich plates when subjected to thermal and mechanical loads. There have not been any studies looking into the detrimental impact of voids on the buckling behavior of FG sandwich plates. Based on the four integral shear deformation theory, a methodical solution for the thermomechanical buckling analysis of imperfect FG sandwich plate has been performed in the current work. The current displacements field is simplified and contains only four unknowns compared to five or more in the similar models and ensures the zero shear stresses at the top and bottom surfaces of the FG sandwich plates based on the hyperbolic warping function in order to avoid the introduction of correction factors. The effect of the porosity in the materials properties is considered because of the possibility of the appearance of porosity in the micro-void form due to the difference of solidification temperature of the (ceramic/metal) constituents in the manufacturing phase. Even, uneven, logarithmic uneven and linear uneven porosity distributions are considered in order to include porosity in the sandwich plate's upper and lower FGM faces and core. This study also includes sandwich plates using type-A and type-B FGM. Considerations are made for both a graded and a uniform temperature rise. Here, power-law FGM is adopted. Temperature independence of the material characteristics is assumed [58, 59]. The Navier method is used to solve the governing equations, which are derived from the idea of minimum total potential energy. By contrasting computed results with those from the existing literature, the validity of the proposed theory was established. The thermomechanical buckling of FG sandwich plates was computed numerically while taking into account the effects of geometrical parameters, porosity coefficient and porosity distribution model.

2 Theoretical formulations

2.1 Geometry and concept of FG sandwich plate

2.1.1 Sandwich plate Type-A

Figure 1 illustrates how the face sheets in type-A sandwich plates are functionally graded across thickness while the sandwich core is homogeneous. The type-A sandwich plate's ceramic volume fraction is provided by [24]:

$$\begin{aligned}
 V^{(1)} &= \left(\frac{z - h_0}{h_1 - h_0} \right)^p \quad z \in [h_0, h_1] \\
 V^{(2)} &= 1 \quad z \in [h_1, h_2] \\
 V^{(3)} &= \left(\frac{z - h_3}{h_2 - h_3} \right)^p \quad z \in [h_2, h_3]
 \end{aligned} \tag{1}$$

2.1.2 Sandwich plate Type-B

As shown in Fig. 1, type-B sandwich plates have uniform face sheets but functionally graded core layers that vary in thickness. The following is the amount of ceramics of sandwich plate type-B [24]:

$$\begin{aligned} V^{(1)} &= 0 \quad z \in [h_0, h_1] \\ V^{(2)} &= \left(\frac{z - h_1}{h_2 - h_1} \right)^p \quad z \in [h_1, h_2] \\ V^{(3)} &= 1 \quad z \in [h_2, h_3] \end{aligned} \quad (2)$$

2.2 Porosity distribution models

By employing Voigt's model and taking into account the power law, the effective material parameters of the FG sandwich plate are determined. Four even and uneven porosity models are taken into account in the current work to account for the porosity in FG faces or cores of FG sandwich plates. The materials that work best for porous FG sandwich plates are given below [60].

2.2.1 Even porosity (Imperfect 1)

$$\text{Type A Sandwich Plate} \begin{cases} \Gamma_1(z) = (\Gamma_c - \Gamma_m)V^{(1)} + \Gamma_m(T) - \frac{\xi}{2}(\Gamma_c + \Gamma_m) \\ \Gamma_2(z) = (\Gamma_c - \Gamma_m)V^{(2)} + \Gamma_m(T) \end{cases} \quad (3)$$

$$\text{Type B Sandwich Plate} \begin{cases} \Gamma_3(z) = (\Gamma_c - \Gamma_m)V^{(3)} + \Gamma_m(T) - \frac{\xi}{2}(\Gamma_c + \Gamma_m) \\ \Gamma_1(z) = (\Gamma_c - \Gamma_m)V^{(1)} + \Gamma_m(T) \\ \Gamma_2(z) = (\Gamma_c - \Gamma_m)V^{(2)} + \Gamma_m(T) - \frac{\xi}{2}(\Gamma_c + \Gamma_m) \\ \Gamma_3(z) = (\Gamma_c - \Gamma_m)V^{(3)} + \Gamma_m(T) \end{cases} \quad (4)$$

2.2.2 Uneven porosity (Imperfect 2)

$$\text{Type A Sandwich Plate} \begin{cases} \Gamma_1(z) = (\Gamma_c - \Gamma_m)V^{(1)} + \Gamma_m(T) - \frac{\xi}{2}(\Gamma_c + \Gamma_m) \left[1 - \frac{|2z - (z_0 + z_1)|}{z_1 - z_0} \right] \\ \Gamma_2(z) = (\Gamma_c - \Gamma_m)V^{(2)} + \Gamma_m(T) \\ \Gamma_3(z) = (\Gamma_c - \Gamma_m)V^{(3)} + \Gamma_m(T) - \frac{\xi}{2}(\Gamma_c + \Gamma_m) \left[1 - \frac{|2z - (z_2 + z_3)|}{z_3 - z_2} \right] \end{cases} \quad (5)$$

$$\text{Type B Sandwich Plate} \begin{cases} \Gamma_1(z) = (\Gamma_c - \Gamma_m)V^{(1)} + \Gamma_m(T) \\ \Gamma_2(z) = (\Gamma_c - \Gamma_m)V^{(2)} + \Gamma_m(T) - \frac{\xi}{2}(\Gamma_c + \Gamma_m) \left[1 - \frac{|2z - (z_1 + z_2)|}{z_2 - z_1} \right] \\ \Gamma_3(z) = (\Gamma_c - \Gamma_m)V^{(3)} + \Gamma_m(T) \end{cases} \quad (6)$$

2.2.3 Uneven porosities (Imperfect 3)

$$\text{Type A Sandwich Plate} \begin{cases} \Gamma_1(z) = (\Gamma_c - \Gamma_m)V^{(1)} + \Gamma_m(T) - \log\left(1 + \frac{\xi}{2}\right)(\Gamma_c + \Gamma_m) \left[1 - \frac{|2z - (z_0 + z_1)|}{z_1 - z_0} \right] \\ \Gamma_2(z) = (\Gamma_c - \Gamma_m)V^{(2)} + \Gamma_m(T) \\ \Gamma_3(z) = (\Gamma_c - \Gamma_m)V^{(3)} + \Gamma_m(T) - \log\left(1 + \frac{\xi}{2}\right)(\Gamma_c + \Gamma_m) \left[1 - \frac{|2z - (z_2 + z_3)|}{z_3 - z_2} \right] \end{cases} \quad (7)$$

$$\text{Type B Sandwich Plate} \begin{cases} \Gamma_1(z) = (\Gamma_c - \Gamma_m)V^{(1)} + \Gamma_m(T) \\ \Gamma_2(z) = (\Gamma_c - \Gamma_m)V^{(2)} + \Gamma_m(T) - \log\left(1 + \frac{\xi}{2}\right)(\Gamma_c + \Gamma_m) \left[1 - \frac{|2z - (z_1 + z_2)|}{z_2 - z_1} \right] \\ \Gamma_3(z) = (\Gamma_c - \Gamma_m)V^{(3)} + \Gamma_m(T) \end{cases} \quad (8)$$

2.2.4 Linear uneven porosities (Imperfect 4)

$$\text{Type A Sandwich Plate} \begin{cases} \Gamma_1(z) = (\Gamma_c - \Gamma_m)V^{(1)} + \Gamma_m(T) - \frac{\xi}{2}(\Gamma_c + \Gamma_m) \left[1 - \frac{z - z_0}{z_0 - z_1} \right] \\ \Gamma_2(z) = (\Gamma_c - \Gamma_m)V^{(2)} + \Gamma_m(T) \\ \Gamma_3(z) = (\Gamma_c - \Gamma_m)V^{(3)} + \Gamma_m(T) - \frac{\xi}{2}(\Gamma_c + \Gamma_m) \left[1 - \frac{z - z_3}{z_2 - z_3} \right] \end{cases} \quad (9)$$

$$\text{Type B Sandwich Plate} \begin{cases} \Gamma_1(z) = (\Gamma_c - \Gamma_m)V^{(1)} + \Gamma_m(T) \\ \Gamma_2(z) = (\Gamma_c - \Gamma_m)V^{(2)} + \Gamma_m(T) - \frac{\xi}{2}(\Gamma_c + \Gamma_m) \left[1 - \frac{z - z_1}{z_1 - z_2} \right] \\ \Gamma_3(z) = (\Gamma_c - \Gamma_m)V^{(3)} + \Gamma_m(T) \end{cases} \quad (10)$$

2.3 Kinematics and strains

The indeterminate integrals are used to reconstruct the conventional five shear deformation theory, reducing the number of variables to just four. It is shown how the generalized displacement field looks like [24]:

$$\begin{aligned} u(x, y, z, t) &= u_0(x, y, t) - z \frac{\partial w_0}{\partial x} + f(z)\phi_x(x, y, t) \\ v(x, y, z, t) &= v_0(x, y, t) - z \frac{\partial w_0}{\partial y} + f(z)\phi_y(x, y, t) \end{aligned} \quad (11)$$

$$w(x, y, z, t) = w_0(x, y, t)$$

where u_0 ; v_0 ; w_0 , ϕ_x , ϕ_y are five unknown displacements of the mid-plane of the plate, $f(z)$ denotes shape function representing the variation of the transverse shear strains and stresses within the thickness. By considering that $\phi_x = \int \theta(x, y)dx$ and $\phi_y = \int \theta(x, y)dy$, the displacement field of the present model can be expressed in a simpler form as:

$$\begin{aligned} u(x, y, z, t) &= u_0(x, y, t) - z \frac{\partial w_0}{\partial x} + k_1 f(z) \int \theta(x, y, t) dx \\ v(x, y, z, t) &= v_0(x, y, t) - z \frac{\partial w_0}{\partial y} + k_2 f(z) \int \theta(x, y, t) dy \end{aligned} \quad (12)$$

$$w(x, y, z, t) = w_0(x, y, t)$$

The current higher-order shear deformation plate theory is obtained in this paper by setting [61]:

$$f(z) = h \sinh\left(\frac{z}{h}\right) - z \cosh\left(\frac{1}{2}\right) \quad (13)$$

It can be seen that the displacement field in Eq. (12) introduces only four unknowns (u_0, v_0, w_0 and θ). The nonzero von Karman strains associated with the displacement field in Eq. (12) are:

$$\begin{Bmatrix} \varepsilon_x \\ \varepsilon_y \\ \gamma_{xy} \end{Bmatrix} = \begin{Bmatrix} \varepsilon_x^0 \\ \varepsilon_y^0 \\ \gamma_{xy}^0 \end{Bmatrix} + z \begin{Bmatrix} k_x^b \\ k_y^b \\ k_{xy}^b \end{Bmatrix} + f(z) \begin{Bmatrix} k_x^s \\ k_y^s \\ k_{xy}^s \end{Bmatrix}, \quad \begin{Bmatrix} \gamma_{yz} \\ \gamma_{xz} \end{Bmatrix} = g(z) \begin{Bmatrix} \gamma_{yz}^0 \\ \gamma_{xz}^0 \end{Bmatrix} \quad (14)$$

where

$$\begin{Bmatrix} \varepsilon_x^0 \\ \varepsilon_y^0 \\ \gamma_{xy}^0 \end{Bmatrix} = \begin{Bmatrix} \frac{\partial u_0}{\partial x} + \frac{1}{2} \left(\frac{\partial w_0}{\partial x} \right)^2 \\ \frac{\partial v_0}{\partial x} + \frac{1}{2} \left(\frac{\partial w_0}{\partial y} \right)^2 \\ \frac{\partial u_0}{\partial y} + \frac{\partial v_0}{\partial x} + \left(\frac{\partial w_0}{\partial x} \right) \left(\frac{\partial w_0}{\partial y} \right) \end{Bmatrix}, \quad \begin{Bmatrix} k_x^b \\ k_y^b \\ k_{xy}^b \end{Bmatrix} = \begin{Bmatrix} -\frac{\partial^2 w_0}{\partial x^2} \\ -\frac{\partial^2 w_0}{\partial y^2} \\ -2\frac{\partial^2 w_0}{\partial x \partial y} \end{Bmatrix} \quad (15a)$$

$$\begin{Bmatrix} k_x^s \\ k_y^s \\ k_{xy}^s \end{Bmatrix} = \begin{Bmatrix} k_1 \theta \\ k_2 \theta \\ k_1 \frac{\partial}{\partial y} \int \theta dx + k_2 \frac{\partial}{\partial x} \int \theta dy \end{Bmatrix}, \quad \begin{Bmatrix} \gamma_{yz}^0 \\ \gamma_{xz}^0 \end{Bmatrix} = \begin{Bmatrix} k_2 \int \theta dy \\ k_1 \int \theta dx \end{Bmatrix} \quad (15b)$$

and

$$g(z) = \frac{df(z)}{dz} \quad (16)$$

The integrals defined in the above equations shall be resolved by a Navier type method and can be written as follows:

$$\frac{\partial}{\partial y} \int \theta dx = A' \frac{\partial^2 \theta}{\partial x \partial y}, \quad \frac{\partial}{\partial x} \int \theta dy = B' \frac{\partial^2 \theta}{\partial x \partial y}, \quad \int \theta dx = A' \frac{\partial \theta}{\partial x}, \quad \int \theta dy = B' \frac{\partial \theta}{\partial y} \quad (17)$$

where the coefficients A' and B' are expressed according to the type of solution used. In this case via Navier, therefore, A' , B' , k_1 and k_2 are expressed as follows:

$$A' = -\frac{1}{\alpha^2}, \quad B' = -\frac{1}{\beta^2}, \quad k_1 = \alpha^2, \quad k_2 = \beta^2 \quad (18)$$

where α and β are defined in expression (31).

For the n -th layer, the stress–strain relationships that take into account thermal effects can be expressed as:

$$\begin{Bmatrix} \sigma_x \\ \sigma_y \\ \tau_{yz} \\ \tau_{xz} \\ \tau_{xy} \end{Bmatrix}^{(n)} = \begin{Bmatrix} \sigma_x^0 \\ \sigma_y^0 \\ \tau_{yz}^0 \\ \tau_{xz}^0 \\ \tau_{xy}^0 \end{Bmatrix}^{(n)} + \begin{Bmatrix} \sigma_x^T \\ \sigma_y^T \\ \tau_{yz}^T \\ \tau_{xz}^T \\ \tau_{xy}^T \end{Bmatrix}^{(n)} = \begin{bmatrix} C_{11} & C_{12} & 0 & 0 & 0 \\ C_{12} & C_{22} & 0 & 0 & 0 \\ 0 & 0 & C_{44} & 0 & 0 \\ 0 & 0 & 0 & C_{55} & 0 \\ 0 & 0 & 0 & 0 & C_{66} \end{bmatrix}^{(n)} \begin{Bmatrix} \varepsilon_x \\ \varepsilon_y \\ \gamma_{yz} \\ \gamma_{xz} \\ \gamma_{xy} \end{Bmatrix}^{(n)} - \alpha \Delta T \begin{Bmatrix} 1 \\ 1 \\ 0 \\ 0 \\ 0 \end{Bmatrix}^{(n)}, \quad (n = 1, 2, 3) \quad (19)$$

Stiffness coefficients, C_{ij} , can be expressed as [22]:

$$C_{11}^{(n)} = C_{22}^{(n)} = \frac{E^{(n)}(z)}{1 - \nu^2}, \quad (20.a)$$

$$C_{12}^{(n)} = \nu C_{11}^{(n)}, \quad (20.b)$$

$$C_{44}^{(n)} = C_{55}^{(n)} = C_{66}^{(n)} = \frac{E^{(n)}(z)}{2(1 + \nu)}, \quad (20.c)$$

2.4 Governing equations

The minimum total potential energy principle, which may be expressed as follows, is employed in this work [61].

$$\delta(U + U_e) = 0 \quad (21)$$

$$U = \frac{1}{2} \int_V \left[\sigma_x^0 \varepsilon_x + \sigma_y^0 \varepsilon_y + \tau_{xy}^0 \delta \gamma_{xy} + \tau_{yz}^0 \delta \gamma_{yz} + \tau_{xz}^0 \delta \gamma_{xz} \right] dV + \frac{1}{2} \int_V \left[\sigma_x^T \left(\frac{\partial w}{\partial x} \right)^2 + \sigma_y^T \left(\frac{\partial w}{\partial y} \right)^2 \right] dV \quad (22)$$

Table 1 Material properties [62]

	Al	Ti-6Al-4V	ZrO ₂	Al ₂ O ₃
Young's modulus (GPa)	70	66.2	244.27	380
Poisson's ratio	0.3	0.3	0.3	0.3
Coefficient of thermal expansion (10 ⁻⁶ /K)	23	10.3	12.766	

The calculation of the external force's potential energy uses [62]:

$$U_e = \frac{1}{2} \int_V \left[N_x^0 \left(\frac{\partial w}{\partial x} \right)^2 + N_y^0 \left(\frac{\partial w}{\partial y} \right)^2 \right] dV \quad (23)$$

where N_x^0 and N_y^0 depict dispersed, compressive, x- and y-directional forces (per unit length) in a plane.

By substituting Eqs. (14) and (19) into Eq. (21), the following can be derived:

$$\begin{aligned} \delta u_0 : \frac{\partial N_x}{\partial x} + \frac{\partial N_{xy}}{\partial y} &= 0 \\ \delta v_0 : \frac{\partial N_{xy}}{\partial x} + \frac{\partial N_y}{\partial y} &= 0 \\ \delta w_0 : \frac{\partial^2 M_x^b}{\partial x^2} + 2 \frac{\partial^2 M_{xy}^b}{\partial x \partial y} + \frac{\partial^2 M_y^b}{\partial y^2} + \bar{N} + \bar{N}^T &= 0 \\ \delta \theta : -k_1 M_x^s - k_2 M_y^s - (k_1 A' + k_2 B') \frac{\partial^2 M_{xy}^s}{\partial x \partial y} + k_1 A' \frac{\partial S_{xz}^s}{\partial x} + k_2 B' \frac{\partial S_{yz}^s}{\partial y} + \bar{N} + \bar{N}^T &= 0 \end{aligned} \quad (24)$$

where the stress resultants N , M and S are defined by

$$\left(N_i, M_i^b, M_i^s \right) = \int_{-h/2}^{h/2} (1, z, f) \sigma_i dz, \quad (i = x, y, xy) \quad \text{and} \quad \left(S_{xz}^s, S_{yz}^s \right) = \int_{-h/2}^{h/2} g (\tau_{xz}, \tau_{yz}) dz \quad (25)$$

And

$$\bar{N} = N_x^0 \frac{\partial^2 (w_0)}{\partial x^2} + N_y^0 \frac{\partial^2 (w_0)}{\partial y^2} \quad (26)$$

$$\bar{N}^T = -N_x^T \frac{\partial^2 (w_0)}{\partial x^2} - N_y^T \frac{\partial^2 (w_0)}{\partial y^2} \quad (27)$$

In which [62]:

$$\left\{ \begin{matrix} N_x^T \\ N_y^T \end{matrix} \right\} = \sum_{n=1}^3 \int_{h_{n-1}}^{h_n} \left\{ \begin{matrix} (C_{11} + C_{12}) \alpha T \\ (C_{11} + C_{12}) \alpha T \end{matrix} \right\}^{(n)} dz \quad (28)$$

2.5 Temperature field

2.5.1 Temperature increase that is uniform

The temperature of the FG sandwich plate is uniformly raised from its initial temperature T_i to the desired temperature T_f in this scenario as the sandwich plate buckles. $\Delta T = T_f - T_i$ is the temperature increment.

Table 2 Dimensionless type-A square sandwich plate critical buckling load \bar{N}_0

p	References	\bar{N}_0					
		1-0-1	2-1-2	2-1-1	1-1-1	2-2-1	1-2-1
0	Zenkour [12]	6.5030	6.5030	6.5030	6.5030	6.5030	6.5030
	Neves et al. [22]	6.5025	6.5025	6.5025	6.5025	6.5025	6.5025
	Thai et al. [25]	6.4774	6.4774	6.4774	6.4774	6.4774	6.4774
	Li et al. [62]	6.5025	6.5025	6.5025	6.5025	6.5025	6.5025
	Present	6.6392	6.6392	6.6392	6.6392	6.6392	6.6392
1	Zenkour [12]	2.5842	2.9206	3.0973	3.2327	3.4749	3.7531
	Neves et al. [22]	2.5392	2.8651	3.0368	3.1678	3.4027	3.6718
	Thai et al. [25]	2.6190	2.9603	3.1401	3.2701	3.5129	3.7799
	Li et al. [62]	2.5836	2.9200	3.0970	3.2324	3.4747	3.7533
	Present	2.6408	2.9847	3.1653	3.3037	3.5511	3.8356
5	Zenkour [12]	1.3300	1.5220	1.7022	1.7903	2.0564	2.3674
	Neves et al. [22]	1.3234	1.5093	1.6860	1.7707	2.0308	2.3303
	Thai et al. [25]	1.3552	1.5754	1.7636	1.8511	2.1227	2.4192
	Li et al. [62]	1.3291	1.5213	1.7018	1.7898	2.0560	2.3673
	Present	1.3588	1.5557	1.7401	1.8302	2.1024	2.4205
10	Zenkour [12]	1.2448	1.3742	1.5672	1.5973	1.5729	2.1909
	Neves et al. [22]	1.2411	1.3654	1.5347	1.5842	1.8358	2.1090
	Thai et al. [25]	1.2553	1.4200	1.5995	1.6531	1.9133	2.1827
	Li et al. [62]	1.2436	1.3732	1.5459	1.5974	1.8538	2.1400
	Present	1.2710	1.4044	1.5809	1.6368	1.8958	2.1884

Table 3 Dimensionless type-B square sandwich plate critical buckling load \bar{N}_0

a/h	Scheme	References	p				
			0	0.5	1	5	10
5	1-1-1	Nguyen et al. [24]	2.0513	2.2342	2.3333	2.5978	2.6834
		Li et al. [62]	2.8714	2.5362	2.3782	2.1198	2.0769
		Present	2.9225	2.5806	2.4192	2.1540	2.5699
	1-2-1	Nguyen et al. [24]	1.9456	2.2725	2.4387	2.8964	3.0545
		Li et al. [62]	3.3388	2.7432	2.4697	2.0546	1.9894
		Present	3.3968	2.7903	2.5115	2.0857	2.5499
	2-2-1	Nguyen et al. [24]	2.1369	2.5023	2.7056	3.2351	3.4009
		Li et al. [62]	2.5905	2.3186	2.1891	1.9531	1.9031
		Present	2.6368	2.3579	2.2246	1.9798	2.5308
10	1-1-1	Nguyen et al. [24]	2.3508	2.5165	2.6123	2.8848	2.9773
		Li et al. [62]	3.1396	2.7889	2.6288	2.3970	2.3696
		Present	2.8903	2.6309	2.5193	2.3669	2.5312
	1-2-1	Nguyen et al. [24]	2.3095	2.5768	2.7322	3.2063	3.3816
		Li et al. [62]	3.6812	3.0330	2.7447	2.3697	2.3353
		Present	3.7620	3.0995	2.8046	2.4200	2.5419
	2-2-1	Nguyen et al. [24]	2.3928	2.7898	3.0116	3.6028	3.7937
		Li et al. [62]	2.8278	2.5746	2.4660	2.3189	2.2967
		Present	3.7620	3.0995	2.8046	2.4200	2.5396
100	1-1-1	Nguyen et al. [24]	2.4773	2.6308	2.7236	2.9969	3.0918
		Li et al. [62]	3.2397	2.8840	2.7238	2.5054	2.4857
		Present	3.9007	3.2174	2.9172	2.5557	2.5382
	1-2-1	Nguyen et al. [24]	2.4730	2.7015	2.8495	3.3268	3.5087
		Li et al. [62]	3.8104	3.1429	2.8497	2.4965	2.4781
		Present	3.9007	3.2174	2.9172	2.5557	2.5382
	2-2-1	Nguyen et al. [24]	2.4963	2.9038	3.1320	3.7467	3.9476
		Li et al. [62]	2.9161	2.6723	2.5738	2.4723	2.4657
		Present	3.9007	3.2174	2.9172	2.5557	2.5385

Table 4 Type-A square sandwich plate's critical buckling temperature rises T_{cr} under uniform temperature rise

Scheme	p	References	a/h				
			5	10	15	25	50
1-0-1	0.5	Zenkour and Sobhy [63]	2.87276	0.80328	0.36504	0.13294	0.03340
		Li et al. [62]	2.87074	0.80314	0.36501	0.13294	0.03340
		Present	2.74152	0.77311	0.35196	0.12830	0.03224
	2	Zenkour and Sobhy [63]	2.63459	0.71815	0.32462	0.11789	0.02958
		Li et al. [62]	2.63018	0.71783	0.32456	0.11788	0.02958
		Present	2.28841	0.62539	0.28283	0.10274	0.02578
2-1-2	0.5	Zenkour and Sobhy [63]	2.83194	0.79232	0.36010	0.13116	0.03295
		Li et al. [62]	2.83030	0.79220	0.36008	0.13115	0.03295
		Present	2.74152	0.77311	0.35196	0.12830	0.03224
	2	Zenkour and Sobhy [63]	2.39953	0.65098	0.29396	0.10671	0.02677
		Li et al. [62]	2.39637	0.65075	0.29392	0.10670	0.02677
		Present	2.28841	0.62539	0.28283	0.10274	0.02578
1-1-1	0.5	Zenkour and Sobhy [63]	2.83331	0.79463	0.36134	0.13164	0.03308
		Li et al. [62]	2.83224	0.79456	0.36133	0.13164	0.03308
		Present	2.74152	0.77311	0.35196	0.12830	0.03224
	2	Zenkour and Sobhy [63]	2.36195	0.64253	0.29031	0.10541	0.02645
		Li et al. [62]	2.36000	0.64239	0.29029	0.10541	0.02645
		Present	2.28841	0.62539	0.28283	0.10274	0.02578
1-2-1	0.5	Zenkour and Sobhy [63]	2.86992	0.80925	0.36841	0.13430	0.03376
		Li et al. [62]	2.86972	0.80925	0.36841	0.13430	0.03376
		Present	2.77703	0.78734	0.35885	0.13089	0.03290
	2	Zenkour and Sobhy [63]	2.42899	0.66689	0.30189	0.10972	0.02754
		Li et al. [62]	2.42873	0.66687	0.30189	0.10972	0.02754
		Present	2.35398	0.64913	0.29412	0.10695	0.02685

2.5.2 Temperature increase that is graded

The top surface temperature T_t differs from the bottom surface temperature T_b , which varies depending on the plate thickness [35]:

$$T(z) = \Delta T \left(\frac{z}{h} + \frac{1}{2} \right)^n + T_t \quad (29)$$

In which n is the temperature index ($0 < n < \infty$) and $\Delta T = T_t - T_b$ is the buckling temperature difference.

3 Analytical solution

The displacement fields are expressed as a function of the boundary conditions using the Navier technique with simply supported boundaries [62].

$$\begin{Bmatrix} u_0 \\ v_0 \\ w_0 \\ \theta \end{Bmatrix} = \sum_{m=1}^{\infty} \sum_{n=1}^{\infty} \begin{Bmatrix} U_{mn} \cos(\lambda x) \sin(\mu y) \\ V_{mn} \sin(\lambda x) \cos(\mu y) \\ W_{0mn} \sin(\lambda x) \sin(\mu y) \\ \theta_{mn} \sin(\lambda x) \sin(\mu y) \end{Bmatrix} \quad (30)$$

where U_{mn} , V_{mn} , W_{0mn} and θ_{mn} are arbitrary parameters to be determined.

$$\lambda = m\pi/a \quad \text{and} \quad \mu = n\pi/b \quad (31)$$

A system of in-plane compressive stresses that are uniform. N_x^0, N_y^0 and $N_{xy}^0 = 0$ in a thermal environment can be used to calculate FGM sandwich plates' critical buckling loads and temperature increase.

Table 5 Type-B square sandwich plate's critical buckling temperature rises T_{cr} during nonlinear temperature rise

Scheme	p	n	References	a/h				
				5	10	15	25	50
1-0-1	0.5	2	Do and Lee [35]	5.35784	1.46297	0.63750	0.20009	0.01238
			Li et al. [62]	5.36625	1.46432	0.63784	0.20010	0.01235
			Present	5.49462	1.52115	0.66583	0.21084	0.01526
		3	Do and Lee [35]	6.77704	1.85048	0.80636	0.25309	0.01565
			Li et al. [62]	6.78766	1.85219	0.80679	0.25311	0.01562
			Present	6.88462	1.90597	0.83427	0.26417	0.01912
		4	Do and Lee [35]	8.25929	2.25522	0.98272	0.30845	0.01908
			Li et al. [62]	8.27222	2.25729	0.98325	0.30846	0.01904
			Present	8.31191	2.30111	1.00723	0.31894	0.02309
		5	Do and Lee [35]	9.78867	2.67282	1.16470	0.36557	0.02261
			Li et al. [62]	9.80398	2.67527	1.16531	0.36558	0.02257
			Present	9.77017	2.70482	1.18394	0.37490	0.02714
	2	2	Do and Lee [35]	5.35784	1.46297	0.63750	0.20009	0.01238
			Li et al. [62]	5.36625	1.46432	0.63784	0.20010	0.01235
			Present	5.81174	1.67185	0.74216	0.24175	0.02537
		3	Do and Lee [35]	6.77704	1.85048	0.80636	0.25309	0.01565
			Li et al. [62]	6.78766	1.85219	0.80679	0.25311	0.01562
			Present	7.04855	2.02764	0.90010	0.29319	0.03078
		4	Do and Lee [35]	8.25929	2.25522	0.98272	0.30845	0.01908
			Li et al. [62]	8.27222	2.25729	0.98325	0.30846	0.01904
			Present	8.29392	2.38589	1.05914	0.34500	0.03621
		5	Do and Lee [35]	9.78867	2.67282	1.16470	0.36557	0.02261
			Li et al. [62]	9.80398	2.67527	1.16531	0.36558	0.02257
			Present	9.56046	2.75024	1.22088	0.39768	0.04175
2-1-2	0.5	2	Do and Lee [35]	5.45505	1.48364	0.64572	0.20226	0.01205
			Li et al. [62]	5.46373	1.48503	0.64607	0.20227	0.01203
			Present	5.49462	1.52115	0.66583	0.21084	0.01526
		3	Do and Lee [35]	6.94175	1.88799	0.82171	0.25738	0.01534
			Li et al. [62]	6.95278	1.88976	0.82216	0.25739	0.01531
			Present	6.88462	1.90597	0.83427	0.26417	0.01912
		4	Do and Lee [35]	8.48806	2.30855	1.00475	0.31471	0.01875
			Li et al. [62]	8.50153	2.31070	1.00529	0.31473	0.01871
			Present	8.31191	2.30111	1.00723	0.31894	0.02309
		5	Do and Lee [35]	10.07658	2.74059	1.19278	0.37361	0.02226
			Li et al. [62]	10.09256	2.74314	1.19343	0.37363	0.02222
			Present	9.77017	2.70482	1.18394	0.37490	0.02714
	2	2	Do and Lee [35]	5.43958	1.49762	0.65488	0.20728	0.01496
			Li et al. [62]	5.44823	1.49904	0.65525	0.20729	0.01493
			Present	5.81174	1.67185	0.74216	0.24175	0.02537
		3	Do and Lee [35]	6.81619	1.87662	0.82061	0.25973	0.01875
			Li et al. [62]	6.82701	1.87840	0.82107	0.25975	0.01871
			Present	7.04855	2.02764	0.90010	0.29319	0.03078
		4	Do and Lee [35]	8.24945	2.27122	0.99316	0.31435	0.02269
			Li et al. [62]	8.26253	2.27338	0.99372	0.31437	0.02265
			Present	8.29392	2.38589	1.05914	0.34500	0.03621
		5	Do and Lee [35]	9.72967	2.67876	1.17137	0.37075	0.02676
			Li et al. [62]	9.74508	2.68129	1.17203	0.37078	0.02671
			Present	9.56046	2.75024	1.22088	0.39768	0.04175
1-1-1	0.5	2	Do and Lee [35]	5.61588	1.52788	0.66526	0.20871	0.01289
			Li et al. [62]	5.62505	1.52936	0.66565	0.20873	0.01286
			Present	5.49462	1.52115	0.66583	0.21084	0.01526
		3	Do and Lee [35]	7.17052	1.95084	0.84943	0.26648	0.01645
			Li et al. [62]	7.18222	1.95273	0.84992	0.26651	0.01643
			Present	6.88462	1.90597	0.83427	0.26417	0.01912
		4	Do and Lee [35]	8.77713	2.38794	1.03974	0.32619	0.02014
			Li et al. [62]	8.79143	2.39025	1.04034	0.32622	0.02011
			Present	8.31191	2.30111	1.00723	0.31894	0.02309
		5	Do and Lee [35]	10.41987	2.83488	1.23434	0.37490	0.02391
			Li et al. [62]	10.43684	2.83761	1.23506	0.38724	0.02387
			Present	9.77017	2.70482	1.18394	0.38728	0.02714

Table 5 continued

Scheme	p	n	References	a/h				
				5	10	15	25	50
	2	2	Do and Lee [35]	5.5788	1.54041	0.67549	0.21523	0.01728
			Li et al. [62]	5.56691	1.54193	0.67590	0.21525	0.01726
			Present	5.81174	1.67185	0.74216	0.24175	0.02537
	3	3	Do and Lee [35]	6.92118	1.91826	0.84118	0.26802	0.02152
			Li et al. [62]	6.93240	1.92015	0.84168	0.26805	0.02149
			Present	7.04855	2.02764	0.90010	0.29319	0.03078
	4	4	Do and Lee [35]	8.33175	2.30921	1.01262	0.32265	0.02591
			Li et al. [62]	8.34523	2.31148	1.01322	0.32268	0.02587
			Present	8.29392	2.38589	1.05914	0.34500	0.03621
	5	5	Do and Lee [35]	9.78507	2.71201	1.18925	0.37893	0.03043
			Li et al. [62]	9.80089	2.71467	1.18996	0.37897	0.03039
			Present	9.56046	2.75024	1.22088	0.39768	0.04175

Table 6 Type-A square imperfect 1 sandwich plate's dimensionless mechanical load and temperature change

Scheme	ξ	\bar{N}_0	$\hat{N}_{T/2}$	T_{cr}^u	$\hat{T}_{N/2}^u$	T_{cr}^l	$\hat{T}_{N/2}^l$
1-0-1	0	1.5046	0.7523	0.6990	0.3495	1.3476	0.6488
	0.05	1.3674	0.6837	0.7115	0.3558	1.3730	0.66149
	0.1	1.2299	0.6149	0.7219	0.3609	1.3937	0.67195
	0.15	1.0923	0.5462	0.7285	0.3643	1.4070	0.67845
	0.2	0.9544	0.4772	0.7295	0.3648	1.4091	0.67952
2-1-2	0	1.6840	0.8420	0.6335	0.3168	1.2172	0.5836
	0.05	1.5482	0.7741	0.6261	0.3131	1.2021	0.5761
	0.1	1.4121	0.7061	0.6144	0.3072	1.1787	0.56434
	0.15	1.2757	0.6379	0.5975	0.2988	1.1451	0.54752
	0.2	1.1390	0.5695	0.5746	0.2873	1.0992	0.52461
1-1-1	0	1.8728	0.9364	0.6255	0.3127	1.2008	0.5754
	0.05	1.7415	0.8708	0.6131	0.3066	1.1762	0.5631
	0.1	1.6098	0.8049	0.5973	0.2987	1.1447	0.54733
	0.15	1.4778	0.7389	0.5775	0.2888	1.1051	0.5276
	0.2	1.3454	0.6727	0.5533	0.2766	1.0568	0.5034
1-2-1	0	2.2170	1.1085	0.6491	0.3245	1.2483	0.5992
	0.05	2.0985	1.0493	0.6359	0.3179	1.2220	0.58596
	0.1	1.9797	0.9899	0.6205	0.31025	1.1910	0.57049
	0.15	1.8607	0.9304	0.6025	0.30125	1.1550	0.55247
	0.2	1.7413	0.8707	0.5818	0.2909	1.1136	0.53178

Equation (30) can be substituted for Eq. (24), resulting in the following result: Assuming that N_x^0 and N_y^0 have a specific ratio so that $N_x^0 = -N^0$ and $N_y^0 = -\gamma N^0$, one can obtain:

$$\left(\begin{bmatrix} S_{11} & S_{12} & S_{13} & S_{14} \\ S_{12} & S_{22} & S_{23} & S_{24} \\ S_{13} & S_{23} & S_{33} & S_{34} \\ S_{14} & S_{24} & S_{34} & S_{44} \end{bmatrix} \right) - \begin{bmatrix} 0 & 0 & 0 & 0 \\ 0 & 0 & 0 & 0 \\ 0 & 0 & P & 0 \\ 0 & 0 & 0 & 0 \end{bmatrix} - \begin{bmatrix} 0 & 0 & 0 & 0 \\ 0 & 0 & 0 & 0 \\ 0 & 0 & l & 0 \\ 0 & 0 & 0 & 0 \end{bmatrix} = \begin{Bmatrix} 0 \\ 0 \\ 0 \\ 0 \end{Bmatrix} \quad (32)$$

where:

$$\begin{aligned} S_{11} &= (\alpha^2 A_{11} + \beta^2 A_{66}) \\ S_{12} &= \alpha\beta(A_{12} + A_{66}) \\ S_{13} &= -\alpha^3 B_{11} - \alpha\beta^2(B_{12} + 2B_{66}) \\ S_{14} &= \alpha((k_2 B' B_{12}^s + (k_1 A' + k_2 B')B_{66}^s)\beta^2 + k_1 A' B_{11}^s \alpha^2) \\ S_{22} &= (\alpha^2 A_{66} + \beta^2 A_{22}) \\ S_{23} &= -\alpha^2\beta(B_{12} + 2B_{66}) - \beta^3 B_{22} \end{aligned}$$

Table 7 Type-B imperfect 1 square sandwich plate's dimensionless mechanical load and temperature change

Scheme	ξ	\bar{N}_0	$\hat{N}_{T/2}$	T_{cr}^u	$\hat{T}_{N/2}^u$	T_{cr}^l	$\hat{T}_{N/2}^l$
2-1-2	0	2.0571	1.02855	0.75887	0.37944	1.1017	0.53210
	0.05	2.0474	1.0237	0.7684	0.3842	1.1116	0.5371
	0.1	2.0376	1.0188	0.7774	0.3887	1.1208	0.54179
	0.15	2.0275	1.01375	0.7858	0.3929	1.1292	0.54602
	0.2	2.0173	1.00865	0.7936	0.3968	1.1367	0.54686
1-1-1	0	2.0578	1.0289	0.78608	0.39304	1.1401	0.55130
	0.05	2.0384	1.0192	0.7861	0.3931	1.1566	0.5597
	0.1	2.0185	1.00925	0.8178	0.4089	1.1722	0.5656
	0.15	1.9980	0.999	0.8325	0.41625	1.1863	0.5748
	0.2	1.9768	0.9884	0.8462	0.4231	1.1990	0.58125
1-2-1	0	2.0653	1.03265	0.8255	0.41275	1.2015	0.58200
	0.05	2.0276	1.0138	0.8499	0.42495	1.2259	0.59437
	0.1	1.9889	0.99445	0.8734	0.4367	1.2489	0.60602
	0.15	1.9488	0.9744	0.8961	0.44805	1.2697	0.61666
	0.2	1.9073	0.9537	0.9173	0.4586	1.2881	0.6260
2-2-1	0	1.9980	0.9990	0.90574	0.45287	1.3061	0.63452
	0.05	1.9829	0.9915	0.9383	0.46915	1.3501	0.6565
	0.1	1.9673	0.9837	0.9709	0.48545	1.3941	0.6786
	0.15	1.9511	0.9755	1.0035	0.50175	1.4377	0.7005
	0.2	1.9344	0.9676	1.0356	0.5178	1.4805	0.7216

$$\begin{aligned}
S_{24} &= \beta((k_1 A' B_{12}^s + (k_1 A' + k_2 B') B_{66}^s) \alpha^2 + k_2 B' B_{22}^s \beta^2) \\
S_{33} &= (\alpha^4 D_{11} + \beta^4 D_{22} + 2\alpha^2 \beta^2 (D_{12} + 2D_{66})) + K_w + K_s (\alpha^2 + \beta^2) \\
S_{34} &= -(\alpha^4 k_1 A' D_{11}^s + \beta^4 k_2 B' D_{22}^s) - \alpha^2 \beta^2 (k_1 A' + k_2 B') (D_{12}^s + 2D_{66}^s) \\
S_{44} &= \alpha^4 (k_1 A')^2 H_{11}^s + \beta^4 (k_2 B')^2 H_{22}^s + (2k_1 k_2 A' B' H_{12}^s + (k_1 A' + k_2 B')^2 H_{66}^s) \alpha^2 \beta^2 \\
&\quad + \alpha^2 ((k_1 A')^2 F_{55}^s + 2k_1 A' X_{55}^s + A_{55}^s) + \beta^2 ((k_2 B')^2 F_{44}^s + A_{44}^s) \\
P &= N_0 (\lambda^2 + \gamma \mu^2) \\
l &= \lambda^2 N_x^T + \mu^2 N_y^T
\end{aligned} \tag{33}$$

4 Numerical results

This section provides a comparative analysis to support the existing formulation. To adequately understand the thermomechanical buckling of FGM sandwich plates, many results are presented that take into account the effects of volume fraction distribution, geometric factors, mechanical and thermal loads. Table 1 lists the material characteristics for ceramics and metals utilized in the numerical illustrations. Assuming nothing else, $T_t = 25$ K, $\gamma = 1$ and $a/h = 10$.

4.1 Validation study

The following categories are used to conduct the verification investigation: mechanical buckling, thermal buckling and thermomechanical buckling of the two type of FG sandwich plates. The FG sandwich plates are constructed of zirconia (ZrO_2) and titanium (Ti-6Al-4V) for thermal buckling and thermomechanical buckling and aluminum (Al) and alumina (Al_2O_3) for mechanical buckling.

The following relationships are used as comparisons and examples [62]:

$$\bar{N}_0 = \frac{N_0^{cr} a^2}{100h^3 E_0}; \quad T_{cr} = 10^{-3} \Delta T_{cr}$$

where $E_0 = 1$ GPa.

Mechanical load and temperature rise are used as dimensionless parameters [62]:

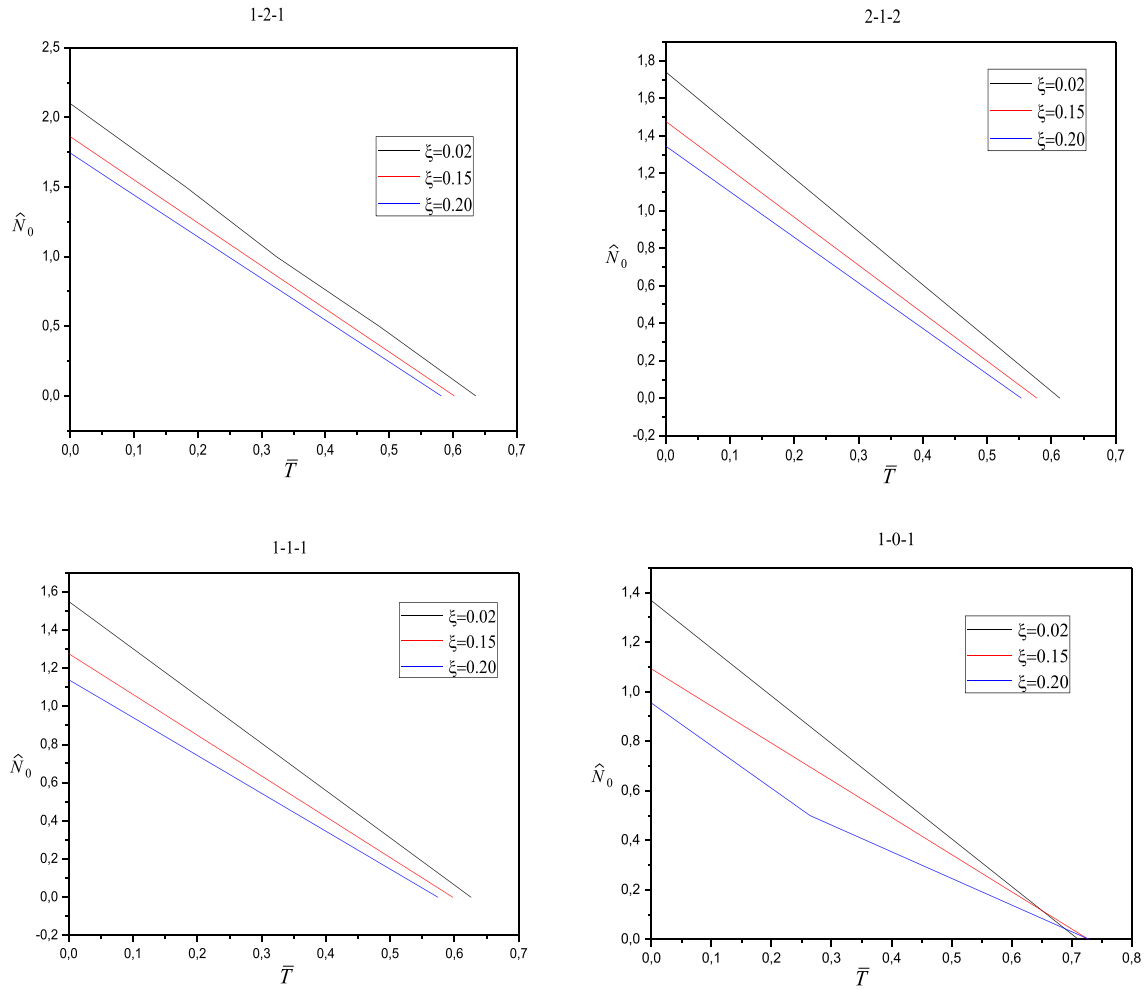


Fig. 2 Temperature increment under uniform temperature rise and the mechanical stress of an imperfect 1 type-A sandwich plate

$$\hat{N}_0 = \frac{N_0^T a^2}{100h^3 E_0}, \quad \hat{T} = \frac{10^{-3} \Delta T}{T_0}$$

where $T_0 = 1 K$.

Tables 2, 3, 4 and 5 display the two type sandwich plates' critical temperature rise and buckling load and for various layer thickness ratios and power indices. As benchmark results, further calculations made using different theories from the literature are also provided. As seen, a good agreement is established for every facet of the buckling problem. It is clear for the type-A, the critical buckling load is biggest one in the case of 1-2-1 because the ceramic layer is thick and has a higher young modulus. We can see also in the same type (A) that the critical buckling loads decrease with the increase of the face's sheets power law because these layers become rich on metal.

Also, the critical buckling temperature is in inverse relation with the side-to-thickness ratio because the plate becomes thin and flexible and a small temperature leads to buckling of the structure. For the second type (B), we can observe for 1-0-1 plate, the power-law index has no influence because the structure does not contain a core, but in the others case (2-1-2 and 1-1-1) the critical buckling temperature rises T_{cr} are in inverse relation with the inhomogeneity index because the core becomes riche on metal and therefore less rigid.

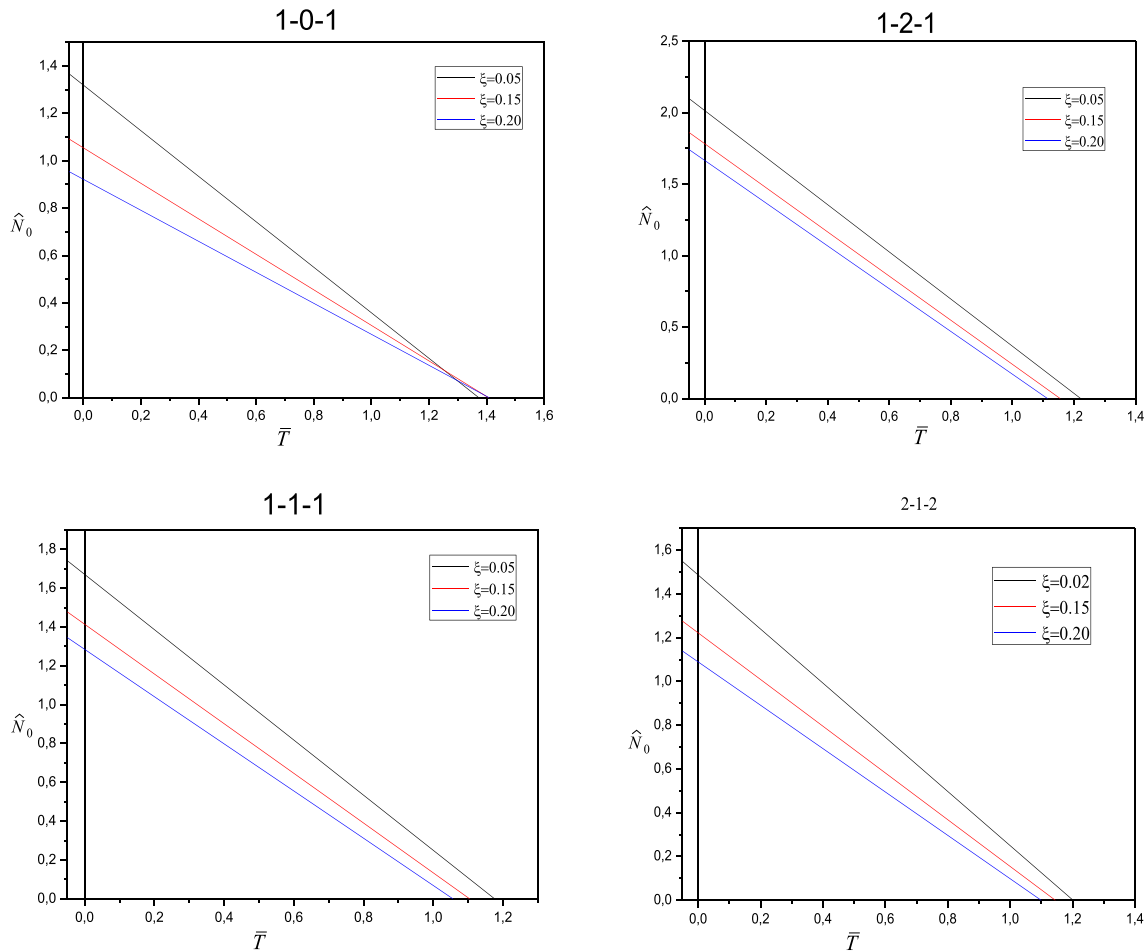


Fig. 3 Temperature increment under linear temperature rise and the mechanical stress of an imperfect 1 type-A sandwich plate

4.2 Imperfect sandwich plate buckling analysis under mechanical and thermal loads

In this illustration, the impact of mechanical and thermal loads on a square, imperfect sandwich plate with simple support is taken into account. It is presumed that the plate buckles when it is subjected to a mechanical load N_0^T and a temperature increase ΔT during both temperature rise (uniform/linear).

First, we determine the dimensionless critical buckling load and temperature increment for imperfect 1 type-A square sandwich plates for $\xi = 0, 0.05, 0.1, 0.15$ and 0.2 with a variety of 2-1-2, 1-0-1, 1-2-1 and 1-1-1 layer thickness ratios under uniform/linear temperature rise using half of the uniform temperature rise critical buckling temperature increment, the mechanical load is then calculated. Additionally, the temperature increase is calculated under a linear and uniform temperature rise by applying half of the critical buckling stress. Table 6 lists these outcomes. The dimensionless critical temperature increase under uniform and linear temperature rise, respectively, are T_{cr}^u and T_{cr}^l . The dimensionless mechanical load under uniform temperature rise is: $\widehat{N}_{T/2}$ using half of the critical buckling temperature increment. Using half of the critical buckling load, the dimensionless temperature increments $T_{N/2}^l$ and $T_{N/2}^u$ are defined as the linear and uniform temperature rise. It has been found that $N_{T/2} = \frac{1}{2}N_0$ and $\widehat{T}_{N/2}^u = \frac{1}{2}T_{cr}^u$, but that $\widehat{T}_{N/2}^l < \frac{1}{2}T_{cr}^l$. It is remarkable that the dimensionless critical mechanical load decrease with the increase of the porosity index because the structures become less rigid. But for critical temperature change, this conclusion is inversed. The same type of work was done for imperfect 1 type-B FGM (Ti-6Al-4V/ZrO₂) sandwich plates under the effect of thermal loads and mechanical loads as observed in Table 7.

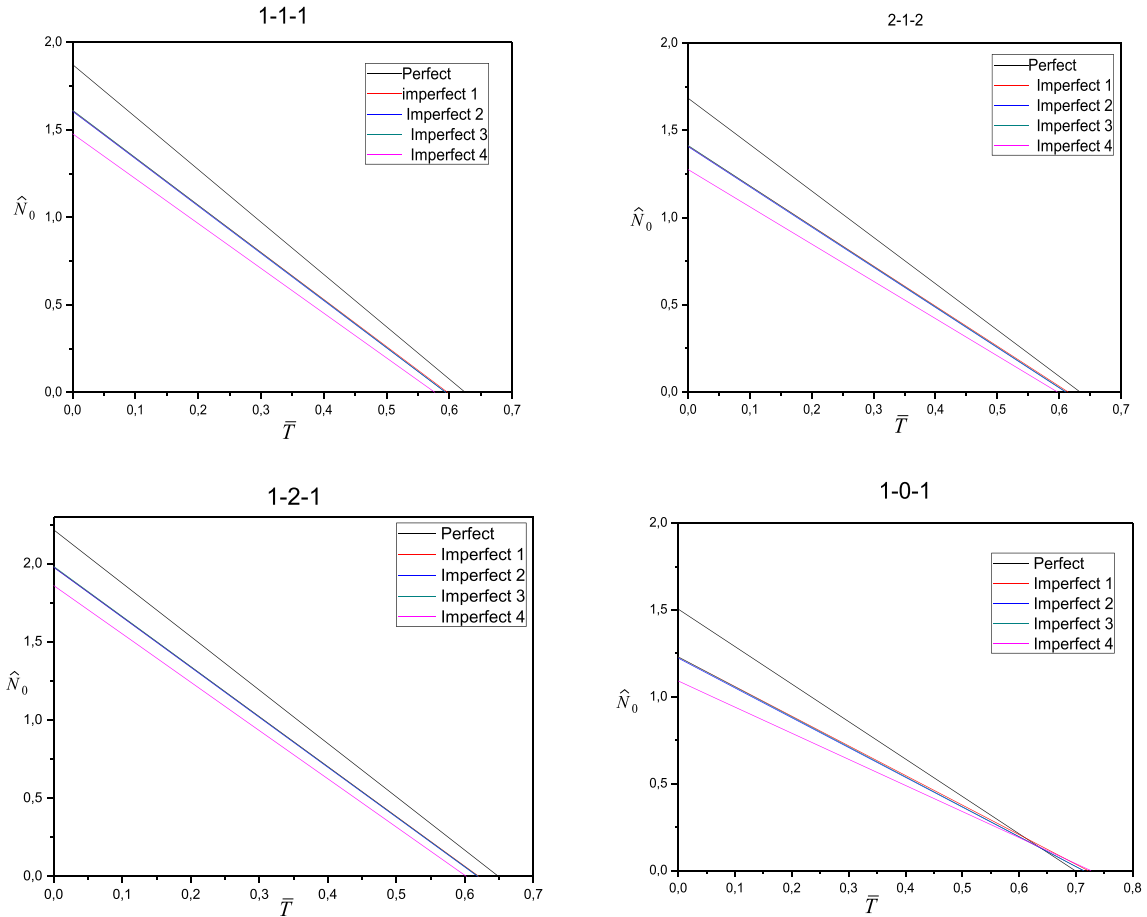


Fig. 4 Temperature increment under uniform temperature rise and the mechanical stress of an imperfect 1,2,3 and 4 type-A sandwich plate

The relationship between temperature increment and mechanical load for the type-A sandwich plates (1-0-1), (2-1-2), (1-1-1) and (1-2-1) is shown in Figs. 2, 3 for $\xi = 0.05, 0.15$ and 0.2 . Figures 2, 3 show that the connection is linear. The mechanical load diminishes as the temperature increment rises. Due to an increase in temperature, compressive internal forces produced, this is to be expected. In Fig. 2, the mechanical load value is zero when the temperature rise reaches its maximum, also the opposite. On the other hand, in Fig. 3, the value of temperature is negative when the mechanical load value reaches its maximum. We can conclude also that the mechanical buckling characteristics are biggest in the case of the 1-2-1 plate type-A, because the thicker layer (core layer) is entirely made of ceramic and therefore the most rigid layer which increases the rigidity of the entire structure.

Analysis of various porosity distributions' effects on the buckling behavior of porous FG sandwich plates has been done in Figs. 4, 5.

The impact of porosity distribution on buckling analysis is examined using models for even, uneven, logarithmic uneven and linear uneven porosity. Porosity distributions' effects on the buckling behavior of porous FG sandwich plates are more prominent in the type-A sandwich plates.

5 Conclusion

The current study has produced an analytical solution for the thermomechanical buckling analysis of porous FG sandwich plates. Using a four-variable integral plate theory, buckling analysis of FG sandwich plates under thermomechanical load was performed. Sandwich plates with homogenous core and face sheets made of FGMs were included for type-A. Sandwich plates had the reverse, while type-B plates. On the basis of the minimal

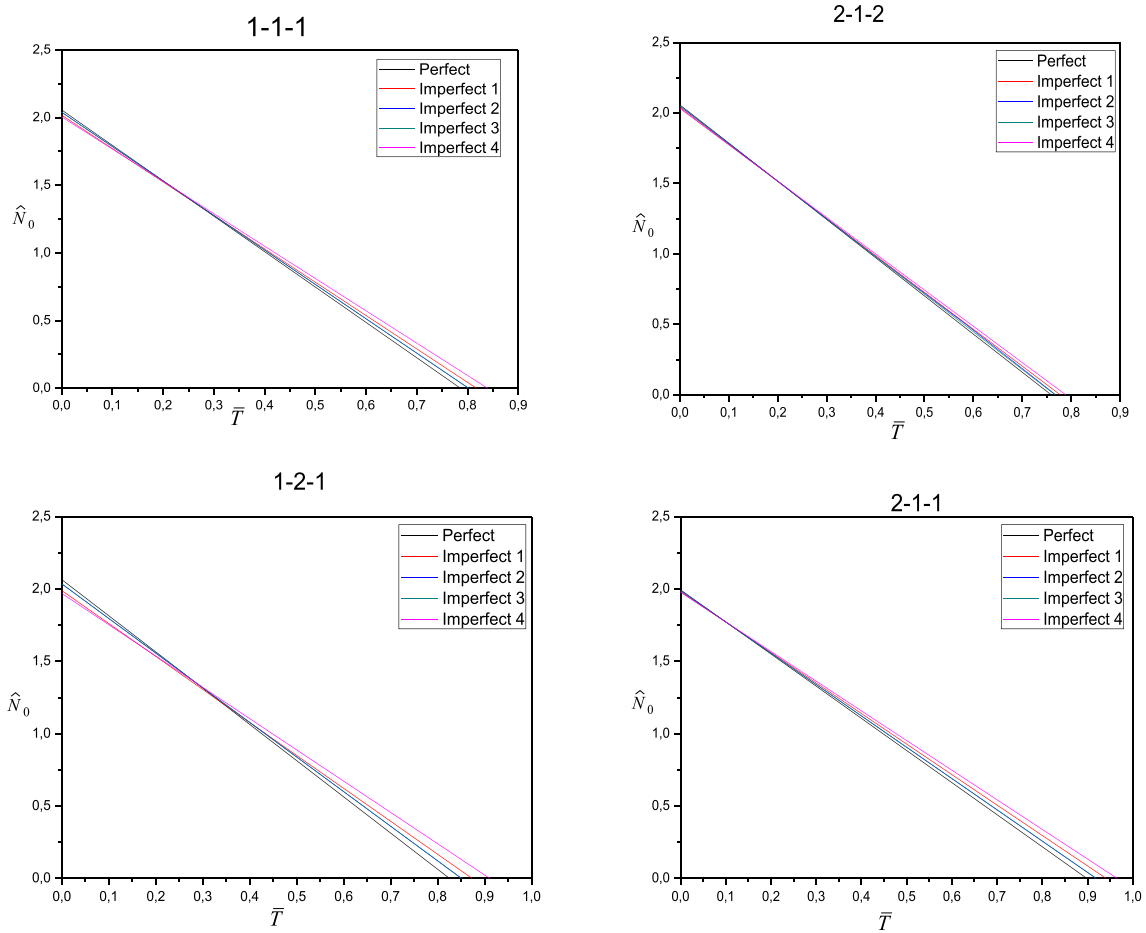


Fig. 5 Temperature increment under uniform temperature rise and the mechanical stress of an imperfect 1, 2, 3 and 4 type-B sandwich plate

total potential energy concept, the governing equations were derived. The Navier method was used to provide the analytical answers for boundary conditions with simple support. To show the accuracy of the proposed theory, the critical buckling load and temperature increase under four temperature rise were computed as well as compared with the results reported in the researches. The thermomechanical buckling behavior of FG sandwich plates was studied while taking the effects of volume fraction distribution, geometrical parameters and porosity into consideration. To study the impact of porosity, four porosity distribution models even (Imperfect 1), uneven (Imperfect 2), logarithmic uneven (Imperfect 3) and linear uneven (Imperfect 4) have been taken into consideration. The obtained results from the present investigation demonstrated the following concluding remarks:

- The critical buckling loads are in inverse relation with face's sheets heterogeneity index because these layers become rich on metal.
- The higher values of the critical buckling load are obtained for 1-2-1 plate (type-A) because the thicker layer (core) is entirely ceramic.
- The increase in the values of the geometry ration leads to decrease the values of the critical buckling temperature.
- The presence of the porosity in the structures has an effect on the critical mechanical and thermal load.

The current finding could serve as a reference point for additional research on FG sandwich plates. The proposed model can be used in the future to examine others type of structures and solve others structural problems [64–85].

Acknowledgements The authors extend their appreciation to the Deanship Scientific Research at King Khalid University for funding this work through large group Research Project under grant number: RGP2/388/45.

Author contributions Imene Laoufi and Fouad Bourada were involved in conceptualization, methodology, investigation, solution approach, writing—original draft preparation and reviewing and editing. Amina Attia was responsible for software, writing—original draft preparation and reviewing and editing. Abdelouahed Tounsi and Murat Yaylaci contributed to conceptualization, reviewing and editing and supervision. Abdeldjebbar Tounsi and Khaled Mohamed Khedher took part in software, solution approach, validation and reviewing and editing. Mohamed Abdelaziz Salem contributed to reviewing and editing.

References

- Birman, V., Kardomateas, G.A.: Review of current trends in research and applications of sandwich structures. *Compos. B Eng.* **142**, 221–240 (2018). <https://doi.org/10.1016/j.compositesb.2018.01.027>
- Garg, A., Belarbi, M.O., Chalak, H.D., Chakrabarti, A.: A review of the analysis of sandwich FGM structures. *Compos. Struct.* **258**, 113427 (2021). <https://doi.org/10.1016/j.compstruct.2020.113427>
- Jha, D.K., Kant, T., Singh, R.K.: A critical review of recent research on functionally graded plates. *Compos. Struct.* **96**, 833–849 (2013). <https://doi.org/10.1016/j.compstruct.2012.09.001>
- Swaminathan, K., Naveenkumar, D.T., Zenkour, A.M., Carrera, E.: Stress, vibration and buckling analyses of FGM plates—a state-of-the-art review. *Compos. Struct.* **120**, 10–31 (2015). <https://doi.org/10.1016/j.compstruct.2014.09.070>
- Alankaya, V., Oktem, A.S.: Static analysis of laminated and sandwich composite doubly-curved shallow shells. *Steel Compos. Struct.* **20**(5), 1043–1069 (2016). <https://doi.org/10.12989/SCS.2016.20.5.1043>
- Mohammadimehr, M., Shahedi, S.: Nonlinear magneto-electro-mechanical vibration analysis of double-bonded sandwich Timoshenko microbeams based on MSGT using GDQM. *Steel Compos. Struct.* **21**(1), 1–36 (2016). <https://doi.org/10.12989/SCS.2016.21.1.001>
- Mohammadimehr, M., Rostami, R., Arefi, M.: Electro-elastic analysis of a sandwich thick plate considering FG core and composite piezoelectric layers on Pasternak foundation using TSDT. *Steel Compos. Struct.* **20**(3), 513–543 (2016). <https://doi.org/10.12989/SCS.2016.20.3.513>
- Sharma, N., Mahapatra, T.R., Panda, S.K., Mehar, K.: Evaluation of vibroacoustic responses of laminated composite sandwich structure using higher-order finite-boundary element model. *Steel Compos. Struct.* **28**(5), 629–639 (2018). <https://doi.org/10.12989/SCS.2018.28.5.629>
- Shahmohammadi, M.A., Azhari, M., Saadatpour, M.M.: Free vibration analysis of sandwich FGM shells using isogeometric B-spline finite strip method. *Steel Compos. Struct.* **34**(3), 361–376 (2020). <https://doi.org/10.12989/SCS.2020.34.3.361>
- Eltaher, M.A., Mohamed, S.A.: Buckling and stability analysis of sandwich beams subjected to varying axial loads. *Steel Compos. Struct.* **34**(2), 241–260 (2020). <https://doi.org/10.12989/SCS.2020.34.2.241>
- Al-Osta, M.A.: Wave propagation investigation of a porous sandwich FG plate under hygrothermal environments via a new first-order shear deformation theory. *Steel Compos. Struct.* **43**(1), 117–127 (2022). <https://doi.org/10.12989/SCS.2022.43.1.117>
- Zenkour, A.M.: A comprehensive analysis of functionally graded sandwich plates: Part I—deflection and stresses. *Int. J. Solids Struct.* **42**, 5224–5242 (2005). <https://doi.org/10.1016/j.ijsolstr.2005.02.016>
- Tornabene, F., Fantuzzi, N., Viola, E., Batra, R.C.: Stress and strain recovery for functionally graded free-form and doubly-curved sandwich shells using higher-order equivalent single layer theory. *Compos. Struct.* **119**, 67–89 (2015). <https://doi.org/10.1016/j.ijsolstr.2005.02.016>
- Fazzolari, F.A.: Natural frequencies and critical temperatures of functionally graded sandwich plates subjected to uniform and non-uniform temperature distributions. *Compos. Struct.* **121**, 197–210 (2015). <https://doi.org/10.1016/j.compstruct.2014.10.039>
- Li, D., Deng, Z., Xiao, H.: Thermomechanical bending analysis of functionally graded sandwich plates using four-variable refined plate theory. *Compos. B Eng.* **106**, 107–119 (2016). <https://doi.org/10.1016/j.compositesb.2016.08.041>
- Li, D., Deng, Z., Chen, G., Ma, T.: Mechanical and thermal buckling of exponentially graded sandwich plates. *J. Therm. Stresses* **41**(7), 883–902 (2018). <https://doi.org/10.1080/01495739.2018.1443407>
- Kashtalyan, M., Menshkykova, M.: Three-dimensional elasticity solution for sandwich panels with a functionally graded core. *Compos. Struct.* **87**(1), 36–43 (2009). <https://doi.org/10.1016/j.compstruct.2007.12.003>
- Brischetto, S.: Classical and mixed advanced models for sandwich plates embedding functionally graded cores. *J. Mech. Mater. Struct.* **4**(1), 13–33 (2009). <https://doi.org/10.2140/jomms.2009.4.13>
- Alibeigloo, A., Liew, K.M.: Free vibration analysis of sandwich cylindrical panel with functionally graded core using three-dimensional theory of elasticity. *Compos. Struct.* **113**, 23–30 (2014). <https://doi.org/10.1016/j.compstruct.2014.03.004>
- Gu, D., Shi, X., Poprawe, R., Bourell, D.L., Setchi, R., Zhu, J.: Material-structure-performance integrated laser-metal additive manufacturing. *Science* (2021). <https://doi.org/10.1126/science.abg1487>
- Sobhani, E., Masoodi, A.R., Ahmadi-Pari, A.R.: Vibration of FG-CNT and FG-GNP sandwich composite coupled conical-cylindrical-conical shell. *Compos. Struct.* **273**, 114281 (2021). <https://doi.org/10.1016/j.compstruct.2021.114281>
- Neves, A.M.A., Ferreira, A.J.M., Carrera, E., Cinefra, M., Roque, C.M.C., Jorge, R.M.N., Soares, C.M.M.: Static, free vibration and buckling analysis of isotropic and sandwich functionally graded plates using a quasi-3D higher-order shear deformation theory and a meshless technique. *Compos. B Eng.* **44**, 657–674 (2013). <https://doi.org/10.1016/j.compositesb.2012.01.089>
- Sobhy, M.: Buckling and free vibration of exponentially graded sandwich plates resting on elastic foundations under various boundary conditions. *Compos. Struct.* **99**, 76–87 (2013). <https://doi.org/10.1016/j.compstruct.2012.11.018>

24. Nguyen, V.H., Nguyen, T.K., Thai, H.T., Vo, T.P.: A new inverse trigonometric shear deformation theory for isotropic and functionally graded sandwich plates. *Compos. B Eng.* **66**, 233–246 (2014). <https://doi.org/10.1016/j.compositesb.2014.05.012>
25. Thai, C.H., Zenkour, A.M., Wahab, M.A., Nguyen-Xuan, H.: A simple four-unknown shear and normal deformations theory for functionally graded isotropic and sandwich plates based on isogeometric analysis. *Compos. Struct.* **139**, 77–95 (2016). <https://doi.org/10.1016/j.compstruct.2015.11.066>
26. Fazzolari, F.A.: Stability analysis of FGM sandwich plates by using variable-kinematics Ritz models. *Mech. Adv. Mater. Struct.* **23**, 1104–1113 (2016). <https://doi.org/10.1080/15376494.2015.1121559>
27. Di Sciuva, M., Sorrenti, M.: Bending, free vibration and buckling of functionally graded carbon nanotube-reinforced sandwich plates, using the extended Refined Zigzag Theory. *Compos. Struct.* **227**, 111324 (2019). <https://doi.org/10.1016/j.compstruct.2019.111324>
28. Rezaiee-Pajand, M., Arabi, E., Masoodi, A.R.: Nonlinear analysis of FG-sandwich plates and shells. *Aerosp. Sci. Technol.* **87**, 178–189 (2019). <https://doi.org/10.1016/j.ast.2019.02.017>
29. Adhikari, B., Dash, P., Singh, B.N.: Buckling analysis of porous FGM sandwich plates under various types nonuniform edge compression based on higher order shear deformation theory. *Compos. Struct.* **251**, 112597 (2020). <https://doi.org/10.1016/j.compstruct.2020.112597>
30. Zenkour, A.M., Sobhy, M.: Thermal buckling of various types of FGM sandwich plates. *Compos. Struct.* **93**, 93–102 (2010). <https://doi.org/10.1016/j.compstruct.2010.06.012>
31. Jalali, S.K., Naei, M.H., Poorsolhjoui, A.: Thermal stability analysis of circular functionally graded sandwich plates of variable thickness using pseudo-spectral method. *Mater. Des.* **31**(10), 4755–4763 (2010). <https://doi.org/10.1016/j.matdes.2010.05.009>
32. Kiani, Y., Bagherizadeh, E., Eslami, M.R.: Thermal and mechanical buckling of sandwich plates with FGM face sheets resting on the Pasternak elastic foundation. *Proc. Inst. Mech. Eng. J. Mech. Eng. Sci.* **226**, 32–41 (2012). <https://doi.org/10.1177/0954406211413657>
33. Kiani, Y., Eslami, M.R.: Thermal buckling and post-buckling response of imperfect temperature-dependent sandwich FGM plates resting on elastic foundation. *Arch. Appl. Mech.* **82**, 891–905 (2012). <https://doi.org/10.1007/s00419-011-0599-8>
34. Sobhy, M.: An accurate shear deformation theory for vibration and buckling of FGM sandwich plates in hygrothermal environment. *Int. J. Mech. Sci.* **110**, 62–77 (2016). <https://doi.org/10.1016/j.ijmecsci.2016.03.003>
35. Do, V.N.V., Lee, C.-H.: Thermal buckling analyses of FGM sandwich plates using the improved radial point interpolation mesh-free method. *Compos. Struct.* **177**, 171–186 (2016). <https://doi.org/10.1016/j.ijmecsci.2016.03.003>
36. Yang, J., Liew, K.M., Kitipornchai, S.: Dynamic stability of laminated FGM plates based on higher-order shear deformation theory. *Comput. Mech.* **33**, 305–315 (2004). <https://doi.org/10.1016/j.ijmecsci.2016.03.003>
37. Wang, Z.X., Shen, H.S.: Nonlinear analysis of sandwich plates with FGM face sheets resting on elastic foundations. *Compos. Struct.* **93**, 2521–2532 (2011). <https://doi.org/10.1016/j.compstruct.2011.04.014>
38. Shen, H.S., Li, S.R.: Postbuckling of sandwich plates with FGM face sheets and temperature-dependent properties. *Compos. B Eng.* **39**, 332–344 (2008). <https://doi.org/10.1016/j.compositesb.2007.01.004>
39. Yaghoobi, H., Yaghoobi, P.: Buckling analysis of sandwich plates with FGM face sheets resting on elastic foundation with various boundary conditions: an analytical approach. *Meccanica* **48**, 2019–2035 (2013). <https://doi.org/10.1007/s11012-013-9720-0>
40. Tung, H.V.: Thermal and thermomechanical postbuckling of FGM sandwich plates resting on elastic foundations with tangential edge constraints and temperature-dependent properties. *Compos. Struct.* **131**, 1028–1039 (2015). <https://doi.org/10.1016/j.compstruct.2015.06.043>
41. Matsunaga, H.: Free vibration and stability of functionally graded plates according to a 2-D higher-order deformation theory. *Compos. Struct.* **82**(4), 499–512 (2008). <https://doi.org/10.1016/j.compstruct.2007.01.030>
42. Shahverdi, H., Barati, M.R.: Vibration analysis of porous functionally graded nanoplates. *Int. J. Eng. Sci.* **120**, 82–99 (2017). <https://doi.org/10.1016/j.ijengsci.2017.06.008>
43. Zhou, J., Moradi, Z., Safa, M., Khadimallah, M.A.: Intelligent modeling to investigate the stability of a two-dimensional functionally graded porosity-dependent nanobeam. *Comput. Concr.* **30**(2), 85–97 (2022). <https://doi.org/10.12989/CAC.2022.30.2.085>
44. Wattanasakulpong, N., Ungbhakorn, V.: Linear and nonlinear vibration analysis of elastically restrained ends FGM beams with porosities. *Aerosp. Sci. Technol.* **32**(1), 111–120 (2014). <https://doi.org/10.1016/j.ast.2013.12.002>
45. Shahsavari, D., Shahsavari, M., Li, L., Karami, B.: A novel quasi-3D hyperbolic theory for free vibration of FG plates with porosities resting on Winkler/Pasternak/Kerr foundation. *Aerosp. Sci. Technol.* **72**, 134–149 (2018). <https://doi.org/10.1016/j.ast.2017.11.004>
46. Salari, E., Ashoori, A., Vanini, S.A.S.: Porosity-dependent asymmetric thermal buckling of inhomogeneous annular nanoplates resting on elastic substrate. *Adv. Nano Res.* **7**(1), 25 (2019). <https://doi.org/10.12989/anr.2019.7.1.025>
47. Karami, B., Ghayesh, M.H.: Vibration characteristics of sandwich microshells with porous functionally graded face sheets. *Int. J. Eng. Sci.* **189**, 103884 (2023). <https://doi.org/10.1016/j.ijengsci.2023.103884>
48. Hadji, L., Avcar, M., Zouatnia, N.: Natural frequency analysis of imperfect FG sandwich plates resting on Winkler-Pasternak foundation. *Mater Today Proc.* **53**, 153–160 (2022). <https://doi.org/10.1016/j.matpr.2021.12.485>
49. Ghazwani, M.H., Alnujaie, A., Vinh, A.M., PH.: Examination of the high-frequency behavior of functionally graded porous nanobeams using nonlocal simple higher-order shear deformation theory. *Acta Mech.* **235**, 2695–2714 (2024). <https://doi.org/10.1007/s00707-024-03858-6>
50. Avcar, M., Hadji, L., Akan, R.: The influence of Winkler-Pasternak elastic foundations on the natural frequencies of imperfect functionally graded sandwich beams. *Geomech. Eng.* **31**, 99–112 (2022). <https://doi.org/10.12989/GAE.2022.31.1.099>
51. Avcar, M., Hadji, L., Tounsi, A.: The static bending analysis of porous functionally graded sandwich beams. In: *Functionally graded structures*, pp. 4–1–4–17. IOP Publishing, Bristol (2023). <https://doi.org/10.1088/978-0-7503-5301-4ch4>
52. Avcar, M., Hadji, L., Civalek, Ö.: The static bending analysis of porous functionally graded sandwich beams. In: *Functionally graded structures*, pp. 8–1–8–16. IOP Publishing, Bristol (2023). <https://doi.org/10.1088/978-0-7503-5301-4ch8>

53. Hadji, L., Avcar, M.: Free vibration analysis of FG porous sandwich plates under various boundary conditions. *J. Appl. Comput. Mech.* **7**, 505–519 (2021). <https://doi.org/10.22055/jacm.2020.35328.2628>
54. Alambeigi, K., Mohammadimehr, M., Bamdad, M.: An analytical study on free vibration of magneto electro micro sandwich beam with FG porous core on Vlasov foundation. *Adv. Nano Res.* **15**, 423–439 (2023). <https://doi.org/10.12989/ANR.2023.15.5.423>
55. Zhang, Y.W., She, G.L.: Nonlinear harmonic resonances of spinning graphene platelets reinforced metal foams cylindrical shell with initial geometric imperfections in thermal environment. *Struct. Eng. Mech.* **88**, 405–417 (2023). <https://doi.org/10.12989/SEM.2023.88.5.405>
56. Safari, M., Mohammadimehr, M., Ashrafi, H.: Forced vibration of a sandwich Timoshenko beam made of GPLRC and porous core. *Struct. Eng. Mech.* **88**, 1–12 (2023). <https://doi.org/10.12989/SEM.2023.88.1.001>
57. Xu, J.Q., She, G.L.: Thermal post-buckling and primary resonance of porous functionally graded beams: effect of elastic foundations and geometric imperfection. *Comput. Concr.* **32**, 543–551 (2023). <https://doi.org/10.12989/CAC.2023.32.6.543>
58. Rezaiee-Pajand, M., Rajabzadeh-Safaei, N., Masoodi, A.R.: An efficient curved beam element for thermo-mechanical nonlinear analysis of functionally graded porous beams. *Structures* **28**, 1035–1049 (2020). <https://doi.org/10.1016/j.istruc.2020.08.038>
59. Rezaiee-Pajand, M., Masoodi, A.R.: Hygro-thermo-elastic nonlinear analysis of functionally graded porous composite thin and moderately thick shallow panels. *Mech. Adv. Mater. Struct.* **42**(4), 594–612 (2022). <https://doi.org/10.1080/15376494.2020.1780524>
60. Sah, S.K., Ghosh, A.: Influence of porosity distribution on free vibration and buckling analysis of multi-directional functionally graded sandwich plates. *Compos. Struct.* **279**, 114795 (2022). <https://doi.org/10.1016/j.compstruct.2021.114795>
61. Soldatos, K.P.A.: transverse shear deformation theory for homogeneous monoclinic plates. *Acta Mech.* **94**, 195–220 (1992). <https://doi.org/10.1007/BF01176650>
62. Li, D., Zhu, H., Gong, X.: Buckling analysis of functionally graded sandwich plates under both mechanical and thermal loads. *Materials* **14**(23), 7194 (2021). <https://doi.org/10.3390/ma14237194>
63. Zenkour, A.M., Sobhy, M.: Thermal buckling of various types of FGM sandwich plates. *Compos. Struct.* **93**, 93–102 (2010). <https://doi.org/10.1016/j.compstruct.2015.11.066>
64. Anil, K.L., Panda, S.K., Sharma, N., Hirwani, C.K., Topal, U.: Optimal fiber volume fraction prediction of layered composite using frequency constraints—a hybrid FEM approach. *Comput. Concr.* **25**(4), 303–310 (2020). <https://doi.org/10.12989/CAC.2020.25.4.303>
65. Turan, M., Uzun Yaylacı, E., Yaylacı, M.: Free vibration and buckling of functionally graded porous beams using analytical, finite element, and artificial neural network methods. *Arch. Appl. Mech.* **93**, 1351–1372 (2023). <https://doi.org/10.1007/s00419-022-02332-w>
66. Madenci, E., Yaghoobi, A., Barut, A.N.: Phan Peridynamics for failure prediction in variable angle tow composites. *Arch. Appl. Mech.* **93**, 93–107 (2023). <https://doi.org/10.1007/s00419-022-02216-z>
67. Civalek, Ö., Uzun, B., Yaylı, M.Ö.: Size-dependent nonlinear stability response of perforated nano/microbeams via Fourier series. *Arch. Appl. Mech.* **93**, 4425–4443 (2023). <https://doi.org/10.1007/s00419-023-02501-5>
68. Sabherwal, P., Belarbi, M.-O., Raman, R., Garg, A., Li, L., Chalak, H.D., Houari, M.S.A., Avcar, M.: Free vibration analysis of laminated sandwich plates using wavelet finite element method. *AIAA J.* **62**, 824–832 (2024). <https://doi.org/10.2514/1.J063364>
69. Sabzi, J., Esfahani, M.R., Ozbakkaloglu, T., Ramezani, A.: The effect of tensile reinforcement on the behavior of CFRP strengthened reinforced concrete beams: an experimental and analytical study. *Steel Compos. Struct.* **46**, 115–132 (2023). <https://doi.org/10.12989/SCS.2023.46.1.115>
70. Malikan, M., Eremeyev, V.A., Sedighi, H.M.: Buckling analysis of a non-concentric double-walled carbon nanotube. *Acta Mech.* **231**, 5007–5020 (2020). <https://doi.org/10.1007/s00707-020-02784-7>
71. Dewangan, H.C., Panda, S.K., Mahmoud, S.R., Harursampath, D., Mahesh, V., Balubaid, M.: Geometrical large deformation-dependent numerical dynamic deflection prediction of cutout borne composite structure under thermomechanical loadings and experimental verification. *Acta Mech.* **233**, 5465–5489 (2022). <https://doi.org/10.1007/s00707-022-03403-3>
72. Huang, Y., Liu, Z., Ma, S., Li, S., Yu, R.: On nonlinear deflection analysis and dynamic response of sandwich plates based on a numerical method. *Steel Compos. Struct.* **47**, 79–90 (2023). <https://doi.org/10.12989/SCS.2023.47.1.079>
73. Ozdemir, O., Esen, I., Ural, H.: Vibration response of rotating carbon nanotube reinforced composites in thermal environment. *Steel Compos. Struct.* **47**, 1–17 (2023). <https://doi.org/10.12989/SCS.2023.47.1.001>
74. Emdadi, M., Mohammadimehr, M., Navi, B.R.: The surface stress effects on the buckling analysis of porous microcomposite annular sandwich plate based on HSDT using Ritz method. *Comput. Concr.* **32**, 439–454 (2023). <https://doi.org/10.12989/CAC.2023.32.5.439>
75. Ding, H.X., Liu, H.B., She, G.L., Wu, F.: Wave propagation of FG-CNTRC plates in thermal environment using the high-order shear deformation plate theory. *Comput. Concr.* **32**, 207–215 (2023). <https://doi.org/10.12989/CAC.2023.32.2.207>
76. Timesli, A.: Prediction of the critical buckling load of SWCNT reinforced concrete cylindrical shell embedded in an elastic foundation. *Comput. Concr.* **26**(1), 53–62 (2020). <https://doi.org/10.12989/CAC.2020.26.1.053>
77. Mehar, K., Panda, S.K.: Nonlinear deformation and stress responses of a graded carbon nanotube sandwich plate structure under thermoelastic loading. *Acta Mech.* **231**, 1105–1123 (2020). <https://doi.org/10.1007/s00707-019-02579-5>
78. Kumar, V., Dewangan, H.C., Sharma, N.: Subrata Kumar Panda Numerical and experimental deflection behavior of damaged doubly curved composite laminated shell structure. *Arch. Appl. Mech.* **92**, 2881–2897 (2022). <https://doi.org/10.1007/s00419-022-02202-5>
79. Ghandourah, E., Hussain, M., Khadimallah, A., Alhawsawi, A., Banoqitah, E.M., Ali, M.R.: Vibration analysis of double-walled carbon nanotubes based on Timoshenko beam theory and wave propagation approach. *Adva. Nano Res.* **14**, 521–525 (2023). <https://doi.org/10.12989/ANR.2023.14.6.521>
80. Shanab, R.A., Mohamed, N.A., Eltaher, M.A., Abdelrahman, A.A.: Dynamic characteristics of viscoelastic nanobeams including cutouts. *Adv. Nano Res.* **14**, 45–65 (2023). <https://doi.org/10.12989/ANR.2023.14.1.045>

81. Ansari, R., Hassani, R., Gholami, Y., Rouhi, H.: Numerical nonlinear bending analysis of FG-GPLRC plates with arbitrary shape including cutout. *Struct. Eng. Mech.* **85**, 147–161 (2023). <https://doi.org/10.12989/SEM.2023.85.2.147>
82. Eltahir, M.A., Shanab, R.A., Mohamed, N.A.: Analytical solution of free vibration of viscoelastic perforated nanobeam. *Arch. Appl. Mech.* **93**, 221–243 (2023). <https://doi.org/10.1007/s00419-022-02184-4>
83. Abouelregal, A.E., Atta, D., Sedighi, H.M.: Vibrational behavior of thermoelastic rotating nanobeams with variable thermal properties based on memory-dependent derivative of heat conduction model. *Arch. Appl. Mech.* **93**, 197–220 (2023). <https://doi.org/10.1007/s00419-022-02110-8>
84. Araujo, L.J., Filho, J.E.A.: Free-vibration and buckling of Mindlin plates using SGN-FEM models and effects of parasitic shear in models performance. *Struct. Eng. Mech.* **87**, 283–296 (2023). <https://doi.org/10.12989/SEM.2023.87.3.283>
85. Sahoo, S., Parida, S.P., Jena, P.C.: Dynamic response of a laminated hybrid composite cantilever beam with multiple cracks & moving mass. *Struct. Eng. Mech.* **87**, 529–540 (2023). <https://doi.org/10.12989/SEM.2023.87.6.529>

Publisher's Note Springer Nature remains neutral with regard to jurisdictional claims in published maps and institutional affiliations.

Springer Nature or its licensor (e.g. a society or other partner) holds exclusive rights to this article under a publishing agreement with the author(s) or other rightsholder(s); author self-archiving of the accepted manuscript version of this article is solely governed by the terms of such publishing agreement and applicable law.